

# The dynamic conductivity and the plasmon profile of Aluminum in the ultra-fast-matter regime.

M.W.C. Dharma-wardana

National Research Council of Canada, Ottawa, Canada, K1A 0R6 \*

(Dated: July 11, 2018)

We use an explicitly isochoric two-temperature theory to analyze recent X-ray laser scattering data for Aluminum in the ultra-fast-matter (UFM) regime up to 6 eV. The observed surprisingly low conductivities are explained by including strong electron-ion scattering effects using the phase shifts calculated via the neutral-pseudo-atom model. The applicability of the Mermin model to UFM is questioned. The static and dynamic conductivity, complex collision frequency and the plasmon line-shape are evaluated within a Born approximation and are in good agreement with experiment.

PACS numbers: 52.25.Os, 52.35.Fp, 52.50.Jm, 78.70.Ck

## INTRODUCTION

*Introduction* - Short-pulsed X-ray photons, e.g., from the Linac Coherent Light Source (LCLS) have begun to provide data in hitherto inaccessible regimes of matter [1, 2]. Such information is of interest in understanding normal matter under extreme conditions [3–6], as well as at new frontiers in high-energy-density matter, astrophysics, fusion physics etc. Such non-equilibrium systems are also produced in semiconductor devices [7]. The theory involves complicated many-body effects and the quantum mechanics of finite-temperature non-equilibrium systems. Standard *ab-initio* methods are inapplicable or computationally prohibitive for this ultra-fast matter (UFM) regime. Extensions of elementary plasma models or Thomas-Fermi models fail badly. Hence computationally simple realistic theories of these systems are essential in the interpretation of experiments on UFM which is a sub-class of warm-dense-matter (WDM) [8]. Here we use a finite- $T$  density-functional theory (DFT) calculation of the electronic charge distribution  $n(r)$  and the ion charge distribution  $\rho(r)$  around an Al ion in the system as the basic ingredient of such a theory. The neutral pseudoatom (NPA) model of Perrot and Dharma-wardana [9, 10] is used in this study.

The LCLS results [1] of the plasmon feature and the dynamic and static conductivities  $\sigma$  of Al up to 6 eV, isochorically held at solid density dramatically improves on the accuracy of the earlier UFM experiments [6, 11]. Surprisingly low static conductivities  $\sigma(0)$  of UFM aluminum are reported in Ref. [1], even at 0.2 eV.

We present two-temperature ( $2T$ ) calculations for isochoric Aluminum. Atomic units (a.u.,  $|e| = \hbar = m_e = 1$ ) are used, and the temperature is in energy units. The ion temperature  $T_i$  is the initial ‘room’ temperature, while only the electron temperature  $T_e$  is raised to 6 eV by the 50 femto-second X-ray pulse. We do not get the gradual decrease of  $\sigma$  with  $T$  found for equilibrium non-isochoric aluminum. Instead, we reproduce the low static conductivities reported in the experiment. The high conductivities of the normal solid and the molten metal

( $T_e = T_i$ ) at low  $T$  are partly attributed to the position of the scattering momentum  $2k_F$  falling within the second minimum in the ion-ion structure factor  $S(q)$ . In an isochoric UFM solid, the ions have no time to adjust to the rapidly heated electrons. The ions (and their bound electrons) remain frozen at their lattice sites, and at  $T_i$ . Hence  $S(q)$ , and the bare electron-ion pseudopotential  $W(q)$  remain essentially unchanged, even up to  $T_e = 6$  eV. The thermal smearing of the Fermi sphere is set by  $f'(k, T_e) = f(k, T_e)(1 - f(k, T_e))$ , where  $f(k, T_e)$  is the electron Fermi function. It’s overlap with the ion-ion  $S(q)$ , and the electron-ion scattering cross section determine the conductivity  $\sigma(0)$  as well as  $\sigma(\omega)$ .

The new experiment provides the profile of the plasmon resonance. We present a simple theory of the momentum relaxation and energy dephasing frequency  $\nu(\omega)$  (also known as the ‘collision frequency’), using a Born approximation constructed to match the  $\omega \rightarrow 0$  conductivity obtained from the NPA phase shifts. The calculated plasmon profile is in good accord with experiment.

*The DFT-NPA model for isochoric UFM Aluminum* - An aluminum nucleus is placed in an electron subsystem and an ion subsystem, within a large sphere ( $R \sim 30$  au.) where all particle correlations reach bulk values as  $r \rightarrow R$ . Hence this ‘neutral-pseudo-atom’ (NPA) is not an ‘average-atom cell-model’ similar to the IN-FERNO model of Lieberman or its improvements [12]. The electron density in the bulk, viz.,  $n_e$  is  $1.81 \times 10^{23}$  electrons/cm<sup>3</sup>, has an electron-sphere radius  $r_s = 2.07$  au. The free-electron pile up  $n_f(r)$  and the scattering phase shifts  $\delta_{kl}$  around the Al nucleus are calculated via the Kohn-Sham equations, using a step-function to mimic the ion-ion pair distribution function  $g(r)$ . This is known to work well for Al [9]. The phase-shifts satisfy the Friedel sum rule, and the DFT uses a finite- $T$  exchange-correlation contribution [13]. All the results in this study follow from the NPA output. The many-ion system is built up via the  $S(q)$  as a superposition of NPAs, using the  $S(q)$  derived within the theory.

At room temperature, this calculation yields an ionization  $Z = 3$  and an ion Wigner-Seitz radius  $r_{ws} \simeq 2.99$

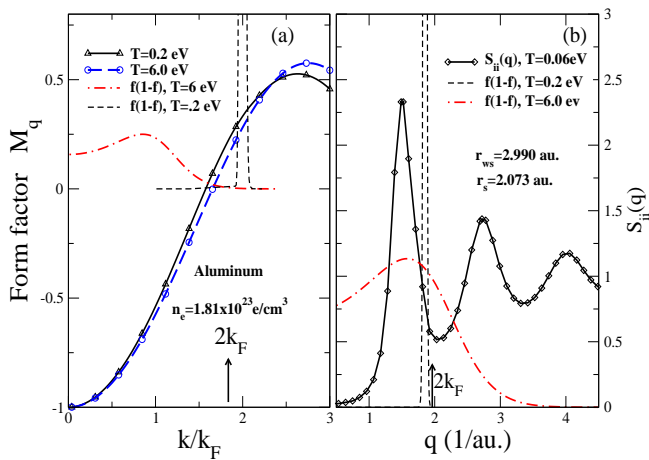


FIG. 1: (Online color). (a) The pseudopotential form factor  $M(q)$  at  $T = 0.2$  eV and 6 eV, and the thermal-smearing functions  $f'(k, T_e) = f(k)(1 - f(k))$ . (b) The overlap of  $S(q)$  and  $f'(k, T_e)$ . The ion  $S(q, T_i)$  with  $T_i = 0.06$  eV.

au. The  $r_{ws}$  is held constant while  $T_e$  is increased, to mimic the isochoric UFM, where as normal solid or liquid Al expands (i.e,  $r_{ws}$  increases) with temperature. A static electron response function  $\chi(q, T_e)$  is constructed, with its local field correction (LFC) satisfying the compressibility sumrule at each temperature. This defines a fully local pseudopotential  $W(q) = n_f(q)/\chi(q, T_e)$ , and an ion-ion pair potential  $U_{ii}(q) = Z^2 V_q - |W(q)|^2 \chi(q)$ . The pseudopotential  $W(q) = -Z V_q M_q$ ,  $V_q = 4\pi/q^2$  is fitted to a Heine-Abarenkov form for convenience. The form factor  $M_q = n_f(q)/n_f^0(q)$  obtained from the NPA is shown in Fig. 1(a) at  $T = 0.2$  and 6 eV. Here  $n_f^0(q)$  is the linear-response charge pileup. This approach is capable of milli-volt accuracy and reproduces even the high-temperature phonons [14] discussed by, e.g., Recoules et al [15] (but phonons do not form during UFM timescales).

The resulting  $U_{ii}(q)$  is used in the modified Hyper-Netted-Chain equation (MHNC) yielding the  $S(q)$  at the ion temperature  $T_i$  (which is the initial temperature of the system at the arrival of the X-ray pulse). Since the initial Al-crystal has an FCC structure, it is sufficient to use the spherically averaged  $S(q)$  taken as a ‘frozen fluid’, say, at 0.06 eV. The latter is the lowest temperature at which the HNC could be converged, since the melting point is  $\simeq 0.082$  eV. The results are insensitive to the use of an  $S(q)$  at 0.06 eV or, say, 0.082 eV. Our MHNC procedure is accurate enough to closely reproduce the experimental  $S(q)$  of normal liquid aluminum [16].

*The complex conductivity  $\sigma(\omega)$*  - The Drude theory with a static  $\nu(0)$  is known to be inadequate for  $\sigma(\omega)$  except at small and high  $\omega$  [19]. Sperling et al [1] have used a Mermin model (diffusion pole) [21] augmented by plasma many-body theory [22] where they combine components of Born (B), Lenard-Balescu (LB) and Gould-DeWitt (GDW)-Mermin (M) approaches in their analy-

sis where  $T_i = T_e$ . The real part of the complex conductivity  $\sigma(\omega) = \sigma_1 + i\sigma_2$ , obtained via B-LB-GDW-M is two orders of magnitude too large compared to experiment, although the imaginary part  $\sigma_2(\omega)$  as well as the plasmon profile are in much better accord. They use several models of  $S(q)$ , point-ion Coulomb potentials as well as pseudopotentials. Since the  $\omega \rightarrow 0$  limit of the  $\sigma(\omega)$  gives a poor  $\sigma(0)$ , they use a Ziman formula with suitable models of  $S(q)$  and pseudopotentials.

In our approach, the ion- $S(q, T_i)$  at  $T_i$  remains intact for all  $T_e$ . We first calculate  $\sigma(0)$  using the electron phase shifts obtained from the NPA and obtain good agreement with experiment. The calculation of  $\sigma(\omega)$  via the phase shifts is more demanding. Instead, since Al is a ‘simple metal’, an Ashcroft pseudopotential  $V_A(r_c)$  specified only by the core radius  $r_c$  that reproduces the  $\sigma(0)$  could be found. This  $r_c$  is consistent with the NPA value. This is used in calculating  $\sigma(\omega)$ . There is no low-frequency ‘diffusion pole’ in the experimental spectra as expected from Mermin theory. Mermin assumes that the ions respond perfectly to the electron-density fluctuations and maintain local charge neutrality. This holds for timescales  $t$  much larger than the electron-ion temperature relaxation time  $\tau_{ei}$  which is many pico-seconds [23] if  $T_i \neq T_e$ , or for timescales significantly larger than phonon timescales if  $T_i = T_e$ . Thus the Mermin model is largely inappropriate for most UFM-WDM systems. Hence we examine a simple RPA-like model where the ions are mere immobile scatterers during the 50 fs signal, and obtain good overall agreement with experiment.

The conductivity  $\sigma(\omega)$  can be expressed via the force-force correlation function as given in standard texts (e.g., Ref. [24] sec. 4.6). If plane waves are used for the free electrons, the limit  $\omega \rightarrow 0$  recovers the Ziman formula. However, if the electron-ion interactions are strong, then the electron response  $\chi(q, \omega)$  and the dynamic conductivity  $\sigma(\omega)$  should be expressed via the electron eigenstates  $\phi(r)_\alpha$  of the system [25, 26]. The NPA provides these, with  $\alpha = n, l$  for core-states, and  $\alpha = k, l; E_{kl} = k^2/2$  for continuum states, with the  $m$  quantum number and spin summed over [25, 26]. The core states give bound-bound transitions, while the bound-continuum and continuum-continuum transitions are also included. If numerical eigenstates  $\phi_\alpha(r)$  are not available, hydrogenic functions can be used within a many-body theory as in Ref. [26]. Such ‘Green-Kubo’ formulae for  $\sigma(\omega)$  usually need heavy numerical codes. Our NPA approach gives a simpler evaluation of comparable accuracy with orders of magnitude rapidity. The corrections beyond the non-interacting response can be expressed as a relaxation frequency  $\nu(\omega) = \nu_1 + i\nu_2$  given in terms of a scattering cross section. The  $\nu$  describes momentum relaxation as well as energy dephasing. This can be expressed via the NPA phase shifts [17, 18]. The real part  $\nu_1(\omega)$  may be

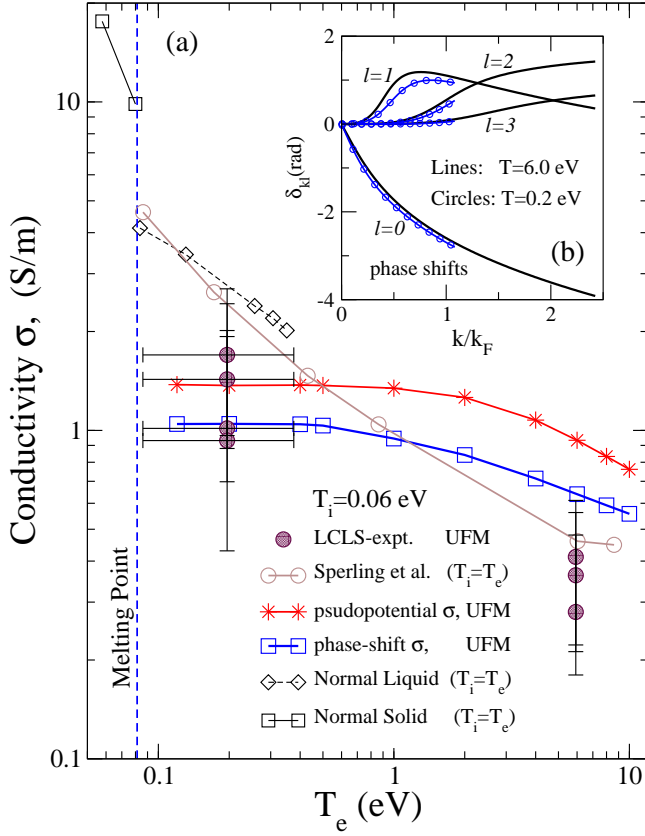


FIG. 2: (Online color) (a) The static conductivity  $\sigma(0)$  of Aluminum. LCLS experiment and the  $\sigma(0)$  from theory for UFM aluminum ( $T_i \neq T_e$ ). Some data for the normal solid and normal liquid are also shown. Sperling et al ( $T_i = T_e$ ) data are a private communication. (b) The NPA phase shifts  $\delta_{kl}$  are shown for  $l = 0-3$ , as a function of  $k/k_F$ .

given as:

$$\nu_1(\omega) = \frac{\Im}{3Z} \sum_{\vec{q}, \vec{k}} q^2 \Sigma(\vec{k}, \vec{q}) S(q) \frac{f(\vec{k}) - f(\vec{k} + \vec{q})}{i\omega(\omega + \epsilon_{\vec{k}} - \epsilon_{\vec{k} + \vec{q}})} \quad (1)$$

$$\Sigma(k, q) = \left| k^{-2} \sum_l (2l+1) e^{i\delta_{kl}} \sin(\delta_{kl}) P_l(\cos\theta) \right|^2 \quad (2)$$

The static limit of Eq. 1 gives:

$$\nu(0) = \frac{1}{3\pi Z T_e} \int_0^\infty f(k) (1 - f(k) k^2 dk F(k)) \quad (3)$$

$$F(k) = \int_0^{2k} q^3 \Sigma(q, k) S(q) dq; \quad q = k(1 - \cos\theta)^{1/2} \quad (4)$$

The original numerical implementation (see appendix, Ref. [17]) has been improved, using up to 38  $l$ -states if needed, using an energy cutoff of  $E_F + 2T_e$ , together with asymptotic corrections. Typical  $\delta_{kl}$  from the NPA are shown in fig. 2(b). Results for  $\sigma(0)$  for isochoric Al, from Eq. 3 covering 0.2 eV to 10 eV are given in Fig. 2(a) while  $\sigma(0)$  up to 100 eV are in Table.1 of Ref. [18]. If the

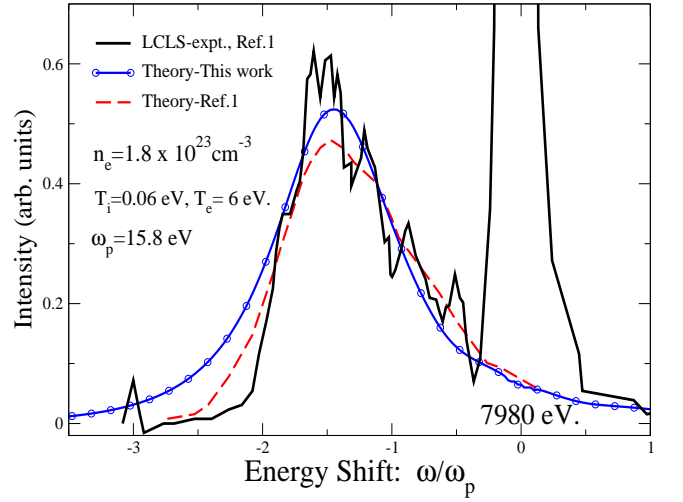


FIG. 3: (Online color) The UFM-aluminum plasmon line-shape at  $T_e = 6$  eV, from experiment and theory.

scattering cross section is evaluated using plane waves (i.e., Born approximation), Eq. 3 reduces to the Ziman formula with the weak pseudo-potential  $W(q) = ZV_q M_q$  (shown in Fig. 1). The Heine-Abarenkov  $W(q)$  gives a higher estimate of  $\sigma(0)$ , while the phase-shift calculation agrees with LCLS.

We replace  $W(q)$  by an Ashcroft pseudopotential  $V_A(q)$  chosen to *reproduce the static conductivity*  $\sigma(0)$ , and use it to evaluate the relaxation frequency  $\nu(\omega)$  in the Born approximation to Eq. (1). Thus,

$$\nu(\omega) = \frac{1}{6\pi^2 Z} \int q^4 |V_A(q)|^2 S(q, T_i) \Delta(q, \omega) dq \quad (5)$$

$$\Delta(q, \omega) = \frac{\{\chi_\epsilon(q, \omega, T_e) - \chi_\epsilon(q, 0, T_e)\}}{i\omega} \quad (6)$$

Eq. (5) is basically Hopfield's expression [19], while modern discussions are found in Refs. [20, 22]. The  $S(q)$  is for the cold ions at  $T_i = 0.06$  eV, as shown in Fig. 1(b).

*The plasmon profile and  $\nu(\omega)$ .* An important result of the LCLS-experiment is the plasmon profile from UFM-Aluminum. We discuss  $T = 6$  eV in detail. Eq. (5) evaluates  $\nu_1(\omega)$  and  $\nu_2(\omega)$  using the  $V_A(r_c)$  pseudopotential. Obtaining  $\nu_1$  via  $\Im\{\chi(q, \omega)\}$  in Eq. 6 and  $\nu_2$  via Kramers-Kronig is computationally convenient. A direct estimate of  $\nu_2$  is also available from Eqs. (5) and (6). The response function  $\chi(q, \omega)$  uses an LFC derived from the finite- $T$  xc-potential [13]. The transverse dielectric function  $\epsilon(q \rightarrow 0, \omega + i\nu(\omega))$  provides the optical scattering cross section  $S_{ee}(q \rightarrow 0, \omega)$ . This is  $\propto \Im\{1/\epsilon(\omega - \nu_2 + i\nu_1)\} n_B(\omega)$  where  $n_B(\omega)$  is a Bose factor at the electron temperature  $T_e$ . Instead of Mermin theory we use the simple RPA-like transverse dielectric function in the  $q \rightarrow 0$  limit. The calculated scattered intensity is shown in Fig. 3. The predicted profile differs on the red wing of the experimental plasmon line shape.

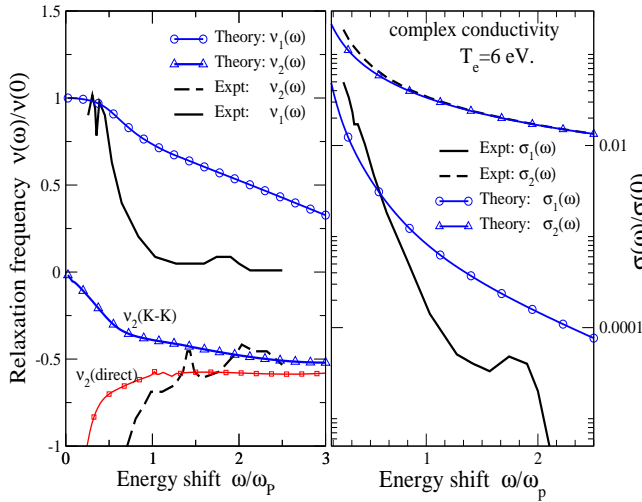


FIG. 4: (Online color) (a) Theory and experiment for the momentum-relaxation frequency  $\nu_1$  and  $\nu_2$  versus the energy shift  $\omega/\omega_p$ .  $\nu_2(\omega)$  calculated from  $\nu_1(\omega)$  via Kramers-Kronig, and via a direct numerical procedure are shown. (b)  $\sigma_1(\omega)$  and  $|\sigma_2(\omega)|$  from experiment and theory.

Since  $V_A(r_c)$  was fitted to the phase-shift  $\sigma$  only at  $\omega = 0$ , this is not surprising.

The relaxation frequency  $\nu(\omega)$  and the conductivity  $\sigma(\omega)$  can be extracted from the experimental  $S(q \rightarrow 0, \omega)$ . We use the experimental  $\nu_1(\omega), \nu_2(\omega)$  of Sperling et al., to test our methods, even though they assumed a Mermin form to extract the data, assuming that the modeling differences fall within the error bars. The experimental  $\nu_1^{ex}$  and  $\nu_2^{ex}$  are compared with the calculated  $\nu_1, \nu_2$  in the figure 4, where the energy shift  $\omega$  is  $\omega_1 - \omega_0$  with  $\omega_0 = 7980$  eV., and hence negative (for the plasmon studied here). The theoretical  $\nu_1$  decays very slowly compared the  $\nu_1^{ex}$ . We expect this to be corrected when a full evaluation using phase shifts is used.

The Drude formula provides  $\sigma(\omega)$  from  $\nu(\omega)$ . Setting  $\varpi = \omega - \nu_2$ ,  $d(\omega) = \nu_1(\omega)^2 + \varpi^2$  we use  $\alpha = \omega_p^2/(4\pi)$ ,  $\sigma_1(\omega) = \alpha\nu_1/d$  and  $\sigma_2(\omega) = \alpha\varpi/d$ . We have recalculated  $\sigma_1, \sigma_2$  from our theoretical  $\nu_1, \nu_2$  given in Fig. 4(a), and from the experimental  $\nu_1, \nu_2$  at  $T=6$  eV given in Fig. 3 of the supplementary material of Ref. [1]. The resulting  $\sigma_1(\omega), \sigma_2(\omega)$  are displayed in Fig. 4(b). Note that although  $\sigma_2(\omega)$  is expected to tend to zero as  $\omega \rightarrow 0$ , this happens only quite close to  $\omega = 0$  because of the strong negativity seen in both experimental and theoretical numbers for  $\nu_2$  (see Fig. 4(a)). Although  $\sigma_1$  is close to the experiment for small- $\omega$ , it begins to differ significantly from experiment as  $\omega$  increases.

In conclusion, the static conductivity calculated using phase-shifted NPA electron eigenfunctions for two-temperature ultra-fast aluminum are in good agreement

with the LCLS data. A simple Born approximation to the dynamic conductivity using a pseudopotential fitted to the theoretical  $\sigma(0)$  provides a good approximation to the plasmon lineshape and the dynamic conductivity obtained from the LCLS experiment. It is argued that the Mermin form is inappropriate for ultrafast matter where the ions have no time to respond. A full calculation of  $\nu(\omega)$  entirely from the phase shifts via Eq. (1) may resolve some of the shortcomings in the present theory.

The author thanks Heide Reinholz, Philipp Sperling and colleagues for their comments.

\* Email address: chandre.dharma-wardana@nrc-cnrc.gc.ca

- [1] P. Sperling et al., Phys. Rev. Lett. **115**, 115001 (2015)
- [2] S. Glenzer and R. Redmer Rev. Mod. Phys. **81**, 1625 (2009)
- [3] Andrew Ng, Int. J. Quant. Chem. **112**, 150 (2012)
- [4] Z. Chen et al., Phys. Rev. Lett. **110**, 135001 (2013)
- [5] Jie Chena et al., Proc. Nat. Acad. Sci., **108** 18887 (2011)
- [6] H. M. Milchberg *et al.* Phys. Rev. Lett. **61**, 2364 (1988).
- [7] M.W.C. Dharma-wardana, Solid State Communications, **86**, 83 (1993)
- [8] F. R. Graziani *et al.* Lawrence Livermore National Laboratory report, USA, LLNL-JRNL-469771 (2011)
- [9] F. Perrot and M.W.C. Dharma-wardana, Phys. Rev. E. **52**, 5352 (1995)
- [10] M. W. C. Dharma-wardana, Contributions to Plasma Physics, **55**, 85 (2015)
- [11] M. W. C. Dharma-wardana and F. Perrot, Phys. Lett. A **163**, 223 (1992)
- [12] Wilson et al., JQSRT **99**, 658-679 (2006)
- [13] F. Perrot and M.W.C. Dharma-wardana, Phys. Rev. B15 **62**, 16536 (2000) *Erratum* **67**, 79901 (2003)
- [14] L. Harbour, M. W. C. Dharma-wardana, D. D. Klug, L. Lewis, Contr. Plasma. Phys. vol. 55, 144-151 (2015)
- [15] V. Recoules et al., Phys. Rev. Lett. **96**, 055503 (2006).
- [16] M. W. C. Dharma-wardana and G. C. Aers, Phys. Rev. B. **28**, 1701 (1983).
- [17] F. Perrot and M. W. C. Dharma-wardana, Phys. Rev. A **36**, 238 (1987).
- [18] F. Perrot and M. W. C. Dharma-wardana, International Journal of Thermophysics, **20**, 1299 (1999)
- [19] Hopfield, Phys. Rev **139**, A419 (1969)
- [20] G. D. Mahan, *Many particle Physics*, Sec. 8.1, Plenum Publishers New York (1981)
- [21] N. D. Mermin, Phys. Rev. B **1**, 2362 (1970)
- [22] H. Reinholz, R. Redmer, G. Röpke and A. Wierling, Phys. Rev. E **62**, 5648 (2000)
- [23] M. W. C. Dharma-wardana, Phys. Rev. E, **64** 035401 (2001)
- [24] G. F. Giuliani et al., *Quantum Theory of the Electron Liquid.*, Sec. 4.6, Cambridge University Press (2005)
- [25] H. Ehrenreich et al., Phys. Rev. **132**, 1918 (1963)
- [26] M. W. C. Dharma-wardana, Physica **92A**, 59 (1978)